Photonic Modal Circulator Using Temporal Refractive-Index Modulation with Spatial Inversion Symmetry

Jiahui Wang[®], Jason F. Herrmann[®], Jeremy D. Witmer, and Amir H. Safavi-Naeini[®] Department of Applied Physics, Stanford University, Stanford, California 94305, USA

Shanhui Fano*

Department of Electrical Engineering, Stanford University, Stanford, California 94305, USA



(Received 26 January 2021; accepted 12 April 2021; published 12 May 2021)

It has been demonstrated that dynamic refractive-index modulation, which breaks time-reversal symmetry, can be used to create on-chip nonreciprocal photonic devices. In order to achieve amplitude nonreciprocity, all such devices moreover require modulations that break spatial symmetries, which adds complexity in implementations. Here we introduce a modal circulator, which achieves amplitude nonreciprocity through a circulation motion among three modes. We show that such a circulator can be achieved in a dynamically modulated structure that preserves mirror symmetry, and as a result can be implemented using only a single standing-wave modulator, which significantly simplifies the implementation of dynamically modulated nonreciprocal devices. We also prove that in terms of the number of modes involved in the transport process, the modal circulator represents the minimum configuration in which complete amplitude nonreciprocity can be achieved while preserving spatial symmetry.

DOI: 10.1103/PhysRevLett.126.193901

Introduction.—The explorations of nonreciprocal photonic structures [1–5] have been of fundamental importance since they offer unique properties, such as optical isolations [6–11], and robust transport [12–15] through disordered systems without the need of symmetry protection, that cannot be achieved in reciprocal systems. Among various paths for creating nonreciprocal photonic structures, the use of dynamically modulated nonmagnetic systems [6–9,16–20], where the refractive index of the system is modulated as a function of time and space, has been of significant recent interest since it offers a route to create nonreciprocal physics using standard optical materials such as silicon [21].

To achieve nonreciprocity through dynamic modulation, both the space and time dependency of the modulation needs to be carefully considered [6–9,16–19]. Certainly, the modulations must have the appropriate temporal waveforms to break reciprocity. In addition, all dynamically modulated on-chip structures considered so far have used a spatial dependency of the modulation that breaks spatial inversion symmetry. For example, for nonreciprocal structures based on traveling wave modulators [8,10], the directionality of the traveling wave breaks spatial inversion symmetry. Similarly, in the optical isolators based on the photonic Aharonov-Bohm effect [6,9], the spatial symmetry is broken with the use of two standing-wave modulators with different modulation phases.

In this Letter, we provide a discussion of the requirement on spatial symmetries in dynamically modulated nonreciprocal systems. We show that breaking spatial inversion symmetry is indeed required in all systems considered previously [6–9] to achieve amplitude nonreciprocity, since only two modes are involved in the transport process. On the other hand, in systems where three modes are involved in the transport process, a nonreciprocal amplitude response is in fact possible even when the modulated system preserves inversion symmetry. As a demonstration of this theoretical understanding, we introduce a nonreciprocal device involving only a single standing-wave modulator, in a structure that preserves mirror symmetry. This design represents a significant simplification for achieving on-chip nonreciprocal devices based on dynamic modulations.

Scattering matrix.—We start with a discussion of the implications of inversion symmetry in the construction of nonreciprocal devices based on dynamic modulations. Suppose the two-port system is harmonically modulated at frequencies that are integer multiples of Ω . In response to incident light at a frequency ω , the steady state consists of multiple sidebands, with the nth sideband at the frequency $\omega + n\Omega$, where n is an integer. At the ith port, we denote the incoming and outgoing amplitudes in the *n*th sideband as $a_{i,n}$ and $b_{i,n}$, respectively, with the normalization chosen such that $|a_{i,n}|^2$ and $|b_{i,n}|^2$ correspond to the photon number flux [6,8], as shown in Fig. 1. The scattering matrix of the dynamically modulated two-port system [4,22] is then

$$\begin{pmatrix} \mathbf{b}_1 \\ \mathbf{b}_2 \end{pmatrix} = \mathbf{S} \begin{pmatrix} \mathbf{a}_1 \\ \mathbf{a}_2 \end{pmatrix}, \tag{1}$$

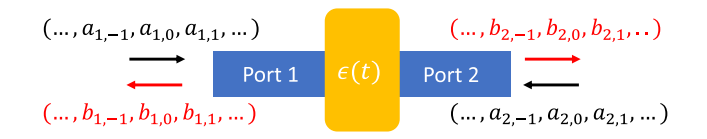


FIG. 1. Dynamically modulated two-port system. The fields at each port consist of multiple frequency sidebands.

where $\mathbf{a}_i = [..., a_{i,-1}, a_{i,0}, a_{i,+1}, ...]^T$ and $\mathbf{b}_i = [..., b_{i,-1}, b_{i,0}, b_{i,+1}, ...]^T$. In what follows, we consider a system with no backscattering, and hence

$$\mathbf{S} = \begin{pmatrix} \mathbf{0} & \mathbf{T}_b \\ \mathbf{T}_f & \mathbf{0} \end{pmatrix}, \tag{2}$$

where \mathbf{T}_f and \mathbf{T}_b are the transfer matrices for the forward and backward directions, respectively.

We define the breaking of the amplitude reciprocity when

$$|\mathbf{S}|_{\odot} \neq |\mathbf{S}^T|_{\odot},$$
 (3)

where $|\cdot|_{\odot}$ represents the absolute-value function operating elementwise on the matrix. From Eqs. (2) and (3), the amplitude nonreciprocity in the system requires that

$$|\mathbf{T}_f|_{\odot} \neq |\mathbf{T}_b^T|_{\odot}.\tag{4}$$

On the other hand, for a structure with either inversion or mirror symmetry that maps one port to the other, we have

$$\mathbf{T}_f = \mathbf{T}_h \equiv \mathbf{T}.\tag{5}$$

Thus, to achieve amplitude nonreciprocity, we must have

$$|\mathbf{T}|_{\odot} \neq |\mathbf{T}^T|_{\odot}.$$
 (6)

For lossless dynamically modulated photonic structures, the photon number flux is conserved [6,8]. Thus, the transfer matrix is unitary [4]:

$$\mathbf{T}\mathbf{T}^{\dagger} = I. \tag{7}$$

In a lossless two-mode system, Eq. (7) implies $|t_{12}| = |t_{21}|$. Thus, $|\mathbf{T}|_{\odot}$ is always symmetric in a two-mode system with inversion or mirror symmetry. This theoretical result is consistent with Refs. [6–9], all of which considered systems with two modes, and utilized modulation schemes that break inversion and mirror symmetry. On the other hand, the derivation above also indicates that it is in fact possible to achieve amplitude nonreciprocity with three modes in each port, using systems with inversion or mirror symmetry, which provides simpler modulation schemes. In what follows, we will provide several examples to illustrate this possibility.

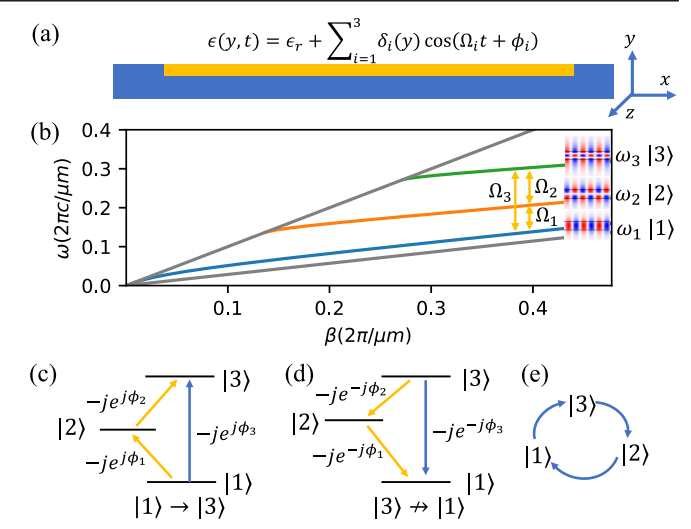


FIG. 2. (a) A slab waveguide design. Blue region represents the static waveguide surrounded by air. The modulation is applied to 1/3 of the waveguide shown as the yellow region. (b) Band structure of the slab waveguide. The waveguide supports three modes. The modulation frequencies Ω_1 , Ω_2 , and Ω_3 are chosen to couple $|1\rangle\leftrightarrow|2\rangle$, $|2\rangle\leftrightarrow|3\rangle$, and $|1\rangle\leftrightarrow|3\rangle$, respectively. Panels (c) and (d) show the phase factors associated with transitions between mode $|1\rangle$ and mode $|3\rangle$. By choosing modulation phases such that $(\phi_1+\phi_2)-\phi_3=\pi/2$, (c) for the up-conversion from mode $|1\rangle\to|3\rangle$, the yellow and the blue pathways constructively interfere, and (d) for the down-conversion from mode $|3\rangle\to|1\rangle$, the two pathways destructively interfere. The transition between mode $|1\rangle$ and $|3\rangle$ is nonreciprocal. (e) Unidirectional circulation among the three modes.

Waveguide implementation.—As a first illustration of the three-mode system as indicated above from the scattering matrix analysis, we consider a slab waveguide that supports three TE (E_z) modes $|1\rangle$, $|2\rangle$, and $|3\rangle$. The band structure of the waveguide is shown in Fig. 2(b). The three different modes have three different frequencies ω_1 , ω_2 , and ω_3 at the same propagation constant β . The waveguide is dynamically modulated with frequencies $\Omega_1 = \omega_2 - \omega_1$, $\Omega_2 = \omega_3 - \omega_2$, and $\Omega_3 = \omega_3 - \omega_1 = \Omega_1 + \Omega_2$ to couple the three modes through direct photonic interband transitions [6,23]. The dynamic modulation is applied uniformly along the x direction with the spatiotemporal profile:

$$\epsilon(y,t) = \epsilon_r + \sum_{i=1}^{3} \delta_i(y) \cos(\Omega_i t + \phi_i),$$
 (8)

where ϵ_r is the static relative permittivity, δ_i is the modulation strength at modulation frequency Ω_i , and ϕ_i is the modulation phase. The modulation is applied only to the upper 1/3 of the waveguide in order to get nonzero coupling coefficients between all three modes. The modulation in Eq. (8) can be implemented by a single standing-wave

modulator where the index modulation is uniform in space along the propagation direction.

With the above modulation profile, the total electric field inside the waveguide can be written as

$$E_z(x, y, t) = e^{-j\beta x} \sum_{n=1}^{3} a_n(x) \hat{E}_{z,n}(y) e^{j\omega_n t},$$
 (9)

where n = 1, 2, 3 represent different modes, $\hat{E}_{z,n}(y)$ is the modal profile of the electric field, and $|a_n(x)|^2$ represents the photon number flux [6,8] for each mode. By substituting Eqs. (8) and (9) into the Maxwell's equation, we can derive the coupled mode theory formalism and calculate the transfer matrix of the system [6,24,25]. Suppose

$$(\phi_1 + \phi_2) - \phi_3 = \pi/2 \tag{10}$$

and

$$C_{12} = C_{23} = C_{13} = \frac{2\pi}{3\sqrt{3}L},$$
 (11)

where $C_{ij} = \frac{1}{8} \int_{-\infty}^{\infty} dy \hat{E}_{z,j} \delta_i \hat{E}_{z,i}^*$ is the coupling coefficients between different modes [6,24] and L is the modulation length. The transfer matrix of the modulated region then has the form:

$$\mathbf{T} = e^{-j\beta L} \begin{pmatrix} 0 & -1 & 0 \\ 0 & 0 & -1 \\ 1 & 0 & 0 \end{pmatrix}, \tag{12}$$

where $e^{-j\beta L}$ is the global propagation phase. The transfer matrix indicates strong amplitude nonreciprocity. Mode $|1\rangle$ input from the left port is converted to mode $|3\rangle$ at the right port. On the other hand, mode $|3\rangle$ input from the right is converted to mode $|2\rangle$, as can be inferred from Eq. (12) as well as the mirror symmetry of the structure.

Equation (12) describes a three-mode circulator [4]. In the standard configuration of a circulator, the modes are those of three single-mode waveguides. Here the modes are the three modes of a single waveguide. Also, in the coupled mode theory we assume only direct transition and ignore indirect transitions that might occur due to the finite length of the modulation region. This assumption is validated by the simulation below.

We validate the coupled mode theory analysis above by performing a first-principles multifrequency finite difference frequency domain (MFFDFD) simulation [26]. In the simulation, the width of the waveguide is $0.4 \mu m$. The waveguide has a relative permittivity $\epsilon_r = 12.25$ and is surrounded by air. Its dispersion relation for the lowest three modes is shown in Fig. 2(b). The modulation region has a length of $L=22.4 \mu m$ and a width that is equal to 1/3 of the waveguide width. We choose $\delta_1 = 0.060\epsilon_r$, $\delta_2=0.044\epsilon_r$, and $\delta_3=0.091\epsilon_r$ such that the coupling coefficients $C_{12}=C_{23}=C_{13}$. The angular frequencies of three modes are $\omega_1 = 2\pi \times 102.9 \text{ THz}$, $\omega_2 = 2\pi \times 161.2$ THz, and $\omega_3 = 2\pi \times 241.7$ THz. The required frequencies of the modulations that drive these transitions can be calculated as $\Omega_1 = 2\pi \times 58.3$ THz, $\Omega_2 = 2\pi \times 80.5$ THz, and $\Omega_3 = 2\pi \times 138.8$ THz. The simulation results as shown in Fig. 3 indicate the amplitude nonreciprocity as predicted from the coupled mode theory formalism. Thus we have demonstrated that to construct a device with amplitude nonreciprocity requires only a single standing-wave modulator. While here for the purpose of reducing computational cost we have used large modulation strengths and frequencies, these modulators can be designed with realistic modulation strength of $\delta/\epsilon \sim 10^{-3}$, and the modulation frequencies in the 100 GHz frequency range [27,28], using the coupled mode theory formalism. Under these more realistic assumptions on the modulations, the transfer matrix of the system still has the form of Eq. (12), but the device has a longer length of 10 mm scale. By choosing the photonic bands of different waveguide modes to be parallel, the operating bandwidth of the modal

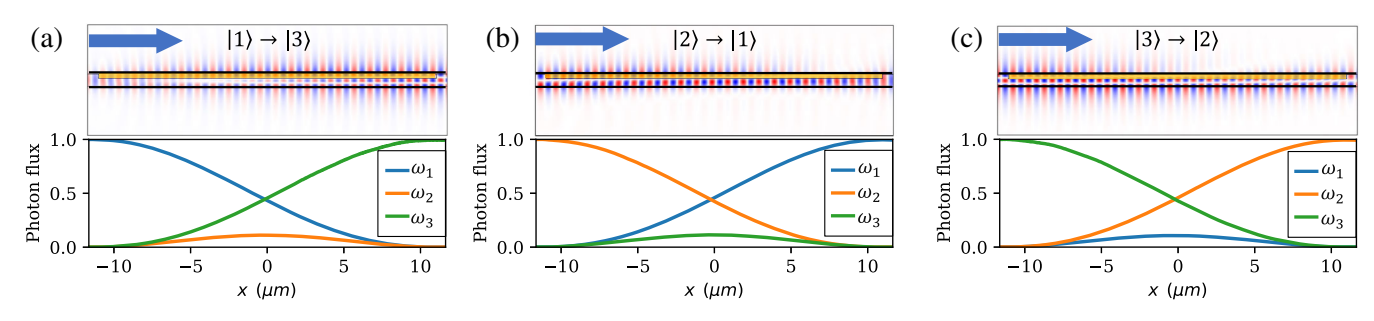


FIG. 3. Waveguide simulation results. The top panels are the normalized E_z field distributions with different input modes from the left port. The solid black lines represent the boundaries of the waveguide and the yellow shaded regions represent the modulation regions. The bottom panels are the normalized photon number flux $|a_n(x)|^2$ as a function of the propagation distance x. The blue, orange, and green lines represent the photon number flux of modes $|1\rangle$, $|2\rangle$, and $|3\rangle$, respectively. Panels (a)–(c) show the complete conversions from $|1\rangle$ to $|3\rangle$, $|2\rangle$ to $|1\rangle$, and $|3\rangle$ to $|2\rangle$, respectively.

circulator can be as broad as on the order of terahertz [29]. Here, for simplicity, we consider lossless system. In the presence of the loss, the coupling constants [i.e., the C_{ij} in Eq. (11)] must dominate over the loss rate of the waveguide in order for the circulator to operate.

Modal circulator.—Both the coupled mode theory and the numerical simulation results as shown in Fig. 3 indicate that the modulated waveguide structure behaves as a modal circulator as described as $|1\rangle \rightarrow |3\rangle \rightarrow |2\rangle \rightarrow |1\rangle$, where each arrow describes an input-output relation. This modal circulator behavior can be understood by examining the phases associated with various photonic transition processes, as plotted in Figs. 2(c) and 2(d). In order for a photon initially in mode $|1\rangle$ to make a transition to mode $|3\rangle$, there are two possible pathways. In the first pathway, the transition can occur through the modulation at frequency Ω_3 , with the associated phase factor of $-ie^{i\phi_3}$. Here ϕ_3 is the modulation phase, and the phase factor -j is a reciprocal phase factor that arises naturally when one computes a scattering matrix S from a Hermitian Hamiltonian **H** through $S = e^{-jHt}$ [24]. In the second pathway, the transition occurs in a two-step process, where the mode $|1\rangle$ first makes a transition to mode $|2\rangle$, and then makes a transition to mode $|3\rangle$. These transitions are associated with the phase factors $-ie^{j\phi_1}$ and $-ie^{j\phi_2}$. With the choice of the parameters in Eqs. (10) and (11), these two pathways constructively interfere, which results in a strong transition from $|1\rangle$ to $|3\rangle$. In contrast, in the reversed direction for the photon to make the transition from $|3\rangle$ to $|1\rangle$, the reciprocal phase factor of -i remains unchanged, but the phases in the exponents which are associated with the modulation phases change the sign, as shown in Fig. 2(d). Hence the two pathways destructively interfere. Repeating the process here for other transitions in this three-mode system, we arrive at the modal circulator behavior as indicated in Fig. 2(e). We note that the reciprocal phase factor of -i plays the role of the reciprocal phase bias [6,24] that allows the nonreciprocity associated with the modulation phase to manifest as amplitude nonreciprocity.

Coupled-ring system.—Based on the discussions above on the mechanisms of modal circulator, we now provide a second implementation using ring resonators, which are more compact as compared to the waveguide design above, but with narrower operating bandwidth. The system consists of three lossless identical ring resonators with resonant frequency of ω_0 , as shown in Fig. 4(a). The rings are arranged in an array with the same edge-to-edge distance d_{rr} , which determines the coupling coefficient μ between the rings. The edge-to-edge distance between the first ring and the waveguide is d_{rw} , which controls the decay rate γ of the mode in the ring to the waveguide. Only the first ring [yellow ring in Fig. 4(a)] is coupled to a straight waveguide which provides the input and output ports.

The static system as described above has three supermodes $|1\rangle$, $|2\rangle$, and $|3\rangle$ with resonant frequencies $\omega_1 = \omega_0 - \sqrt{2}\mu$, $\omega_2 = \omega_0$, and $\omega_3 = \omega_0 + \sqrt{2}\mu$, respectively. All three supermodes have nonzero field components in the first ring. Therefore, one can couple all three modes resonantly by modulating only the first ring with the modulation profile:

$$\epsilon(t) = \epsilon_r + \delta_1 \cos(\Omega t + \phi_1) + \delta_2 \cos(2\Omega t + \phi_2), \tag{13}$$

194.78

 $\omega_0 + \sqrt{2}\mu$

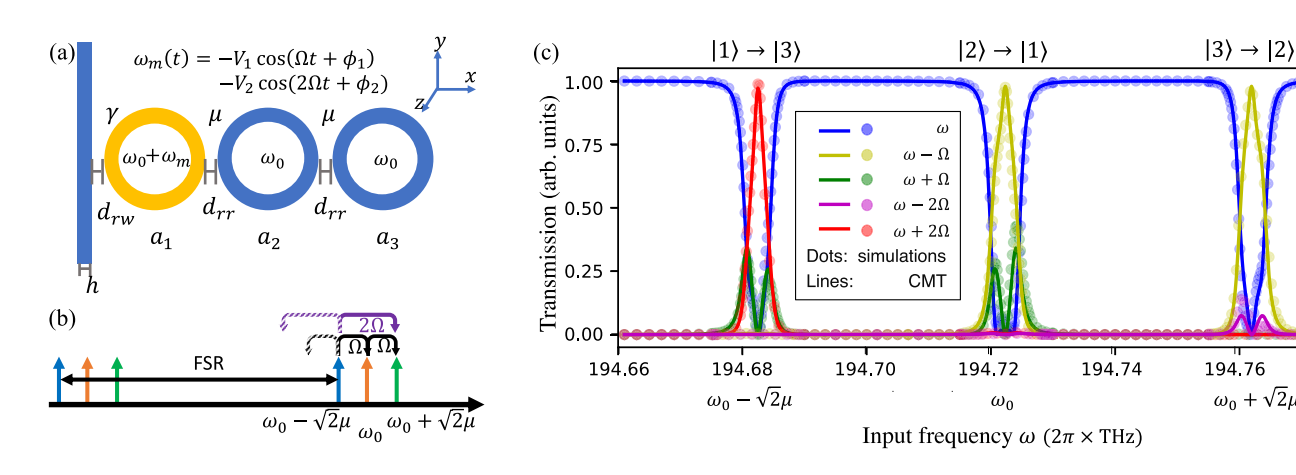


FIG. 4. Coupled-ring system. (a) The coupled-ring system preserves mirror symmetry about the xz plane. The system consists of three identical ring resonators coupled with coefficient μ . Only the yellow ring is coupled to a straight waveguide and is modulated such that its resonant frequency varies as $\omega_0 + \omega_m(t)$. (b) The frequency spectrum for the coupled-ring system. The coupled-ring system supports three supermodes with frequency separation $\sqrt{2}\mu$, which is far smaller than the free spectral range (FSR). (c) Transmission of different frequency components as a function of the input frequency ω . The solid lines are the coupled mode theory (CMT) fitting results and the dots represent the simulation results. When the incident light has frequency $\omega \approx \omega_0 - \sqrt{2}\mu \approx 2\pi \times 194.682$ THz, there is a strong output at $\omega + 2\Omega$, indicating the transition $|1\rangle \rightarrow |3\rangle$. Similarly, the $|2\rangle \rightarrow |1\rangle$ occurs at input frequency around 194.722 THz and the $|3\rangle \rightarrow |1\rangle$ occurs at input frequency around 194.762 THz.

where $\Omega = \sqrt{2}\mu$ describes the fundamental modulation frequency and $\delta_{1,2}$ is the modulation strength in relative permittivity. The resonant frequency of the first ring varies accordingly as

$$\omega(t) = \omega_0 - V_1 \cos(\Omega t + \phi_1) - V_2 \cos(2\Omega t + \phi_2), \quad (14)$$

where $V_{1,2}$ describes the modulation strength in angular frequency. Here we assume that Ω is far smaller than the free spectral range of the ring.

For the incoming field at frequency $\omega \approx \omega_1$ with unit amplitude, we denote the amplitude of the outgoing field at around $\omega + 2\Omega \approx \omega_3$ as t_{31} , since such outgoing field results from photonic transition in the ring resonators from $|1\rangle$ to $|3\rangle$. We can similarly define t_{13} as the transmission from $|3\rangle$ to $|1\rangle$. Similar to the waveguide system, due to the mirror plane symmetry, the difference between the magnitude of t_{13} and t_{31} indicates amplitude nonreciprocity. t_{13} and t_{31} can be calculated analytically with the coupled mode theory [16,24,30,31]. In order to achieve maximum amplitude nonreciprocity, i.e., to have $|t_{31}|=1$ and $|t_{13}|=0$, the modulation must satisfy

$$2\phi_1 - \phi_2 = \pi/2, \qquad V_1 = V_2 = 2\gamma,$$
 (15)

for which case the photon transition in the ring resonator is unidirectional: the transition from $|1\rangle$ to $|3\rangle$ is allowed whereas the transition from $|3\rangle$ to $|1\rangle$ is forbidden. The same condition of Eq. (15) also allows unidirectional photonic transitions for $|2\rangle \rightarrow |1\rangle$ and $|3\rangle \rightarrow |2\rangle$. And thus again, we see that the three supermodes in the ring form a modal circulator similar to the waveguide case.

To verify the analysis above, we perform the MFFDFD simulations [26] and compare the results with the coupled mode theory formalism [24]. In our simulation, three identical ring resonators each have 3.875 μ m inner radius and 4.125 μ m outer radius. The straight waveguide has a width $h = 0.25 \mu m$. The ring-ring and ring-waveguide distances are $d_{rr} = 0.32 \ \mu \text{m}$ and $d_{rw} = 0.26 \ \mu \text{m}$, respectively. The whole structure has relative permittivity $\epsilon_r =$ 12.25 and is surrounded by air. The modulation frequency is $\Omega = 2\pi \times 39.62$ GHz to match the splitting of supermodes. We choose $\phi_1=\pi/2,~\phi_2=\pi/2,~{\rm and}~\delta_1/\epsilon_r=$ $\delta_2/\epsilon_r = 7.14 \times 10^{-5}$ to satisfy the conditions we derived in Eq. (15). The parameters for the modulation should be achievable for state-of-the-art electro-optical modulators [27,28,32–35]. The energy cost of these modulators can be as low as 0.1–10 fJ/bit.

We keep five frequency components $(\omega, \omega \pm \Omega)$ and $\omega \pm 2\Omega$ in the MFFDFD simulations and the coupled mode theory formalism [24], and plot the normalized steady-state transmissions for different frequency components as a function of the input frequency ω in Fig. 4(c). The agreements between the simulations and the theory indicate that the system indeed operates as a modal

circulator within the rings. The bandwidth of the coupled-ring system is limited by the decay rate γ . For the above coupled-ring design, the bandwidth is around 10 GHz. For the lossy ring resonator, the transition rate between various modes must be larger than the total loss rates of the ring resonator in order to maximize the contrast ratio.

Conclusion.—In conclusion, we show that, to achieve amplitude nonreciprocity in dynamically modulated photonic systems, it is necessary to break the spatial inversion symmetry for all previous systems [6–9] where only two modes are involved in the transport process. On the other hand, it is possible to achieve amplitude nonreciprocity with a three-mode system when the spatial inversion symmetry is preserved. We numerically demonstrate the concepts using a three-mode waveguide system and a three-coupled-ring system with the support of the coupled mode theory. Both systems form a modal circulator with only a single standing-wave modulator while preserving the mirror symmetry, which greatly simplify the control and design of on-chip nonreciprocal devices based on dynamic modulations.

The work is supported by a MURI project from the U.S. Air Force of Scientific Research (Grant No. FA9550-18-1-0379). J. F. H. acknowledges support by the National Science Foundation Graduate Research Fellowship Program (Grant No. DGE-1656518). The authors would like to thank Dr. Momchil Minkov, Ms. Zhexin Zhao, Dr. Viktar Asadchy, and Professor Meir Orenstein for helpful discussions.

^{*}shanhui@stanford.edu

^[1] R. J. Potton, Reciprocity in optics, Rep. Prog. Phys. **67**, 717 (2004).

^[2] S. Fan, R. Baets, A. Petrov, Z. Yu, J. D. Joannopoulos, W. Freude, A. Melloni, M. Popović, M. Vanwolleghem, D. Jalas *et al.*, Comment on "Nonreciprocal light propagation in a silicon photonic circuit", Science 335, 38 (2012).

^[3] C. Caloz, A. Alu, S. Tretyakov, D. Sounas, K. Achouri, and Z.-L. Deck-Léger, Electromagnetic Nonreciprocity, Phys. Rev. Applied 10, 047001 (2018).

^[4] I. A. Williamson, M. Minkov, A. Dutt, J. Wang, A. Y. Song, and S. Fan, Integrated nonreciprocal photonic devices with dynamic modulation, Proc. IEEE **108**, 1759 (2020).

^[5] D. Jalas, A. Petrov, M. Eich, W. Freude, S. Fan, Z. Yu, R. Baets, M. Popović, A. Melloni, J. D. Joannopoulos *et al.*, What is — and what is not — an optical isolator, Nat. Photonics 7, 579 (2013).

^[6] K. Fang, Z. Yu, and S. Fan, Photonic Aharonov-Bohm Effect Based on Dynamic Modulation, Phys. Rev. Lett. 108, 153901 (2012).

^[7] H. Lira, Z. Yu, S. Fan, and M. Lipson, Electrically Driven Nonreciprocity Induced by Interband Photonic Transition on a Silicon Chip, Phys. Rev. Lett. 109, 033901 (2012).

- [8] Z. Yu and S. Fan, Complete optical isolation created by indirect interband photonic transitions, Nat. Photonics 3, 91 (2009).
- [9] L. D. Tzuang, K. Fang, P. Nussenzveig, S. Fan, and M. Lipson, Non-reciprocal phase shift induced by an effective magnetic flux for light, Nat. Photonics 8, 701 (2014).
- [10] E. A. Kittlaus, N. T. Otterstrom, P. Kharel, S. Gertler, and P. T. Rakich, Non-reciprocal interband Brillouin modulation, Nat. Photonics 12, 613 (2018).
- [11] L. Bi, J. Hu, P. Jiang, D. H. Kim, G. F. Dionne, L. C. Kimerling, and C. Ross, On-chip optical isolation in monolithically integrated non-reciprocal optical resonators, Nat. Photonics 5, 758 (2011).
- [12] K. Fang, Z. Yu, and S. Fan, Realizing effective magnetic field for photons by controlling the phase of dynamic modulation, Nat. Photonics **6**, 782 (2012).
- [13] M. Hafezi, S. Mittal, J. Fan, A. Migdall, and J. Taylor, Imaging topological edge states in silicon photonics, Nat. Photonics 7, 1001 (2013).
- [14] S. Raghu and F. D. M. Haldane, Analogs of quantum-Hall-effect edge states in photonic crystals, Phys. Rev. A **78**, 033834 (2008).
- [15] Z. Wang, Y. Chong, J. D. Joannopoulos, and M. Soljačić, Observation of unidirectional backscattering-immune topological electromagnetic states, Nature (London) 461, 772 (2009).
- [16] C. W. Peterson, W. A. Benalcazar, M. Lin, T. L. Hughes, and G. Bahl, Strong Nonreciprocity in Modulated Resonator Chains through Synthetic Electric and Magnetic Fields, Phys. Rev. Lett. 123, 063901 (2019).
- [17] N. A. Estep, D. L. Sounas, J. Soric, and A. Alù, Magnetic-free non-reciprocity and isolation based on parametrically modulated coupledresonator loops, Nat. Phys. 10, 923 (2014).
- [18] C. R. Doerr, N. Dupuis, and L. Zhang, Optical isolator using two tandem phase modulators, Opt. Lett. 36, 4293 (2011).
- [19] D. L. Sounas and A. Alù, Angular-momentum-biased nanorings to realize magnetic-free integrated optical isolation, ACS Photonics 1, 198 (2014).
- [20] I. Cardea, D. Grassani, S. J. Fabbri, J. Upham, R. W. Boyd, H. Altug, S. A. Schulz, K. L. Tsakmakidis, and C.-S. Brès, Arbitrarily high time bandwidth performance in a nonreciprocal optical resonator with broken time invariance, Sci. Rep. 10, 15752 (2020).
- [21] G. T. Reed, G. Mashanovich, F. Y. Gardes, and D. Thomson, Silicon optical modulators, Nat. Photonics 4, 518 (2010).
- [22] M. Tymchenko, D. Sounas, and A. Alù, Composite Floquet scattering matrix for the analysis of time-modulated systems, in *Proceedings of the 2017 IEEE International* Symposium on Antennas and Propagation & USNC/URSI National Radio Science Meeting (IEEE, New York, 2017),

- pp. 65–66, http://dx.doi.org/10.1109/APUSNCURSINRSM .2017.8072075.
- [23] J. N. Winn, S. Fan, J. D. Joannopoulos, and E. P. Ippen, Interband transitions in photonic crystals, Phys. Rev. B 59, 1551 (1999).
- [24] See Supplemental Material at http://link.aps.org/supplemental/ 10.1103/PhysRevLett.126.193901 for the explanation of the origin of the reciprocal transition phase and the derivations of the coupled mode theory for waveguide and ring-based systems.
- [25] H. A. Haus, Waves and Fields in Optoelectronics (Prentice-Hall, Englewood Cliffs, NJ, 1984).
- [26] Y. Shi, W. Shin, and S. Fan, Multi-frequency finitedifference frequency-domain algorithm for active nanophotonic device simulations, Optica 3, 1256 (2016).
- [27] C. Wang, M. Zhang, X. Chen, M. Bertrand, A. Shams-Ansari, S. Chandrasekhar, P. Winzer, and M. Lončar, Integrated lithium niobate electro-optic modulators operating at CMOS-compatible voltages, Nature (London) 562, 101 (2018).
- [28] M. He, M. Xu, Y. Ren, J. Jian, Z. Ruan, Y. Xu, S. Gao, S. Sun, X. Wen, L. Zhou, L. Liu, C. Guo, H. Chen, S. Yu, L. Liu, and X. Cai, High-performance hybrid silicon and lithium niobate Mach–Zehnder modulators for 100 Gbit s⁻¹ and beyond, Nat. Photonics 13, 359 (2019).
- [29] Z. Yu and S. Fan, Integrated nonmagnetic optical isolators based on photonic transitions, IEEE J. Sel. Top. Quantum Electron. **16**, 459 (2009).
- [30] W. Suh, Z. Wang, and S. Fan, Temporal coupled-mode theory and the presence of non-orthogonal modes in lossless multimode cavities, IEEE J. Quantum Electron. **40**, 1511 (2004).
- [31] M. Minkov, Y. Shi, and S. Fan, Exact solution to the steady-state dynamics of a periodically modulated resonator, APL Photonics **2**, 076101 (2017).
- [32] M. Zhang, C. Wang, Y. Hu, A. Shams-Ansari, T. Ren, S. Fan, and M. Lončar, Electronically programmable photonic molecule, Nat. Photonics 13, 36 (2019).
- [33] Y. Hu, M. Yu, D. Zhu, N. Sinclair, A. Shams-Ansari, L. Shao, J. Holzgrafe, E. Puma, M. Zhang, and M. Lončar, Reconfigurable electro-optic frequency shifter, arXiv:2005. 09621.
- [34] P. Dong, S. F. Preble, J. T. Robinson, S. Manipatruni, and M. Lipson, Inducing Photonic Transitions between Discrete Modes in a Silicon Optical Microcavity, Phys. Rev. Lett. 100, 033904 (2008).
- [35] L. Chen, Q. Xu, M. G. Wood, and R. M. Reano, Hybrid silicon and lithium niobate electro-optical ring modulator, Optica 1, 112 (2014).